Heat transfer modelling of rail thermite welding

Y Chen[1]*, **F V Lawrence**[2], **C P L Barkan**[2], and **J A Dantzig**[3]
[1]Argonne National Laboratory, Energy Technology Division, Argonne, Illinois, USA
[2]Civil and Environmental Engineering Department, University of Illinois at Urbana-Champaign, Urbana, Illinois, USA
[3]Mechanical and Industrial Engineering Department, University of Illinois at Urbana-Champaign, Urbana, Illinois, USA

The manuscript was received 15 April 2005 and was accepted after revision for publication on 21 March 2006.

DOI: 10.1243/09544097F01505

Abstract: Rail thermite (or Thermit®) welding is a valuable welding technology for the railway industry because of its simplicity, portability, and economy. Using the finite-element method, a heat transfer analysis is conducted in this study. Only the heat transfer by conduction was simulated explicitly in the model, the other thermally significant phenomena were included through the boundary and initial conditions. Despite these simplifications, the model can be used to analyse the thermal conditions during thermite welding with sufficient accuracy. The predicted temperature history, weld deposit, and HAZ profiles were in good agreement with the experimental measurements in laboratory welds. It is found that the weld gap is the most influential welding parameter for rail thermite welding. A wider-gap weld appears to be less sensitive to chance variations in the other welding parameters, and therefore fairly consistent thermal conditions can be obtained.

Keywords: rail thermite welding, heat transfer model, finite-element method analysis

1 INTRODUCTION

Thermite (or Thermit®) welding is a technology that utilizes alumino-thermite reactions to fuse large industrial components [**1**, **2**]. In the railway industry, thermite welding is widely used for the production of field-welded rail joints [**3**]. Its simplicity, economy, and portability make thermite welding an important rail welding technology for railways around the world. Like all fusion welding processes, the quality of thermite welds depends on the thermal conditions during welding. The macro- and microstructure of the weld metal, the weld defect, and the residual stress are all influenced by the thermal history of weldment. Despite the importance of thermal conditions, few studies have focused on thermal analysis of thermite welds. Two earlier investigations involving thermal analysis of thermite welds were carried out by Schroeder and Poirier [**4**] and Jha [**5**]. Both studies focused on the temperature evolution in parent rails and on the post-weld heat treatment, whereas thermal conditions in the weld metal and in the rail immediately adjacent to the weld metal were largely ignored. As the formation of weld defects is closely related to the solidification and cooling process during welding, a good understanding of the heat transfer and the thermal history of the weld metal and the rail end is essential. For this reason, the finite-element method (FEM) is employed to model the thermite welding process and study the temperature evolution during thermite welding. In this article, the FEM thermal model is introduced and calibrated using temperature measurements during laboratory thermite welds. On the basis of this model, the weld defects whose formation mechanisms are sensitive to thermal conditions of welding (such as cold-lap, shrinkage cavity, centreline defect cluster, and microporosity) can be explored. The application of this model in analysing the influence of welding parameters on weld defect formation will be discussed in a subsequent paper.

*Corresponding author: Former graduate student of University of Illinois at Urbana-Champaign. Current address: Argonne National Laboratory, Energy Technology Division, 9700 South Cass Avenue, Argonne, IL 60439, USA. email: yiren_chen@anl.gov

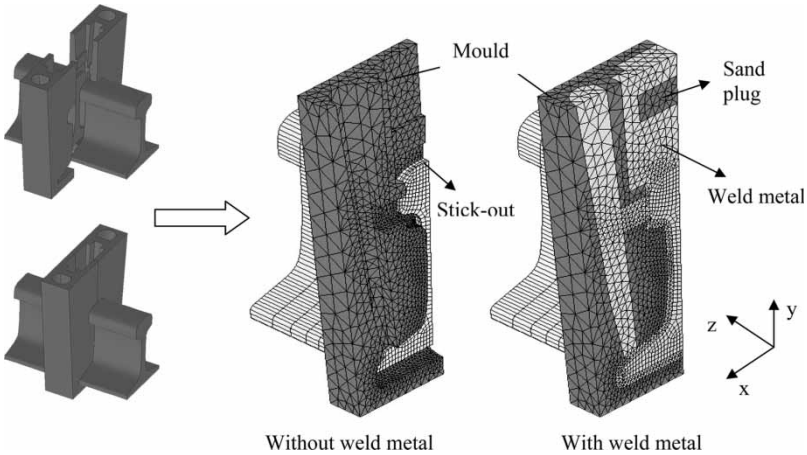

Fig. 1 Model with and without weld metal used in the simulations

2 HEAT TRANSFER MODEL OF RAIL THERMITE WELDING

A typical assembly of rail thermite welding is shown in Fig. 1. Two pieces of slide-on welding mould surround the butted rail ends to form a welding cavity. After securing the mould and sealing the gap between rail and mould, the rail ends and weld mould are preheated with a propane–oxygen flame, and then molten steel is poured into the cavity to fuse the rail ends together. A heat transfer model was developed to analyse thermal history during this process using FIDAP, a finite-element analysis package from Fluent [**6**]. Because of the complex nature of thermite welding, it is difficult to include all the physical phenomena in one model. In this study, only heat conduction, which has the dominant influence on the temperature evolution in thermite welds, was modelled explicitly. The energy balance inside the studied domain is therefore given as

$$\rho C_{\mathrm{p}} \frac{\partial T}{\partial t} = \dot{Q} + \nabla(k \nabla T) \tag{1}$$

where t is the time, $\dot{Q}$ the heat generation rate, ρ the density, and C_{p} the specific heat. The other thermally significant physical processes such as solidification, heat convection, and radiation were included in the model through the material properties, the boundary and initial conditions. A detailed description of these boundary and initial conditions will be given after the model geometry is introduced.

2.1 Model generation

Because of the mirror symmetries about the longitudinal and transverse central planes, only one quarter of the weldment needs to be modelled. The model geometry that includes the shape of the rail, the weld, and the sand mould was built and meshed using GAMBIT, a preprocessor for FIDAP (Fig. 1). The actual dimensions of rail and mould were measured from a 136 lb rail and a standard Thermit SkV* mould. The rail end was not fully covered by the mould in the model. A small portion of rail end passes beyond the mould collar and sticks into the weld chamber. This portion of rail end (referred to as 'stick-out' in Fig. 1) is subjected to the propane–oxygen flame during preheating and is surrounded by weld metal during solidification. The amount of weld metal simulated in the model is the volume of weld cavity and is shaded in light grey in Fig. 1. As the dimensions of the weld mould are fixed for a given weld gap, the length of 'stick-out' will affect the 'effective' weld gap, which is the true distance between two butted rail ends.

An eight-node linear brick element was used to discretize the rail and part of the weld metal. The mesh density was uniform vertically from the rail head to base and gradually increased horizontally from the far end of the rail towards the weld end. A four-node linear tetrahedron element was used to discretize the mould and the rest of weld metal (the geometry of which is more complicated). Again, the mesh density was higher in the weld metal and was gradually reduced in the mould with increasing distance from the weld–mould interface.

2.2 Material properties

Constant densities for the rail steel (7.87 g/cm^3) and the sand mould (1.6 g/cm^3) were assumed for the heat transfer simulations. The conductivities of the steel and the sand mould vary with temperature below the melting point, as shown in Fig. 2 [**7**].

*SkV is a standard short preheating thermite welding procedure.

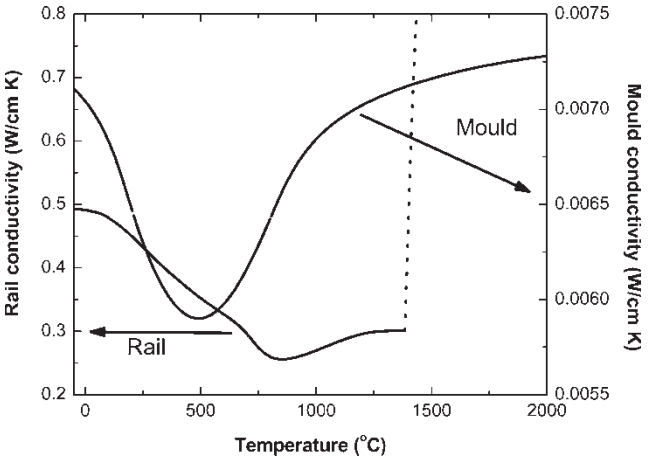

Fig. 2 Thermal conductivities used in the model

As the model does not explicitly include the heat transfer by convection, the effective thermal conductivity of steel was increased by a factor of five when the temperature was higher than the melting point. By doing so, the enhanced heat transfer by convection in liquid metal is taken into account.

Melting, solidification, and solid-state transformations occur during the thermite welding process. There are several ways to include the latent heat released (or absorbed) during these phase transformations. In this study, the latent heat was included through the specific heat term in equation (1). An enthalpy (H) versus temperature (T) curve was first defined in the input file, and then the specific heat was calculated dynamically using the 'enthalpy-specific heat' method provided with FIDAP package [**8**]

$$C_{\mathrm{p}} = \frac{H(T_n) - H(T_{n-1})}{T_n - T_{n-1}} \tag{2}$$

where the subscripts refer to time steps. This method has been proved to be more robust and less sensitive to time step size and mesh density [**9**]. Figure 3 shows the enthalpies of steel and sand mould that were implemented in the heat transfer model. The spikes in the specific heat curves in Fig. 3 represent the discontinuities generated by solidification or solid-state transformation. A linear variation of the enthalpy is assumed within the temperature ranges of phase transformations. The data for specific heat and latent heat of fusion were taken from references [**7**, **10**].

2.3 Boundary and initial conditions

The process of thermite rail welding was divided into two stages in the simulation, i.e. the preheating and tapping stage and the solidification stage. Different

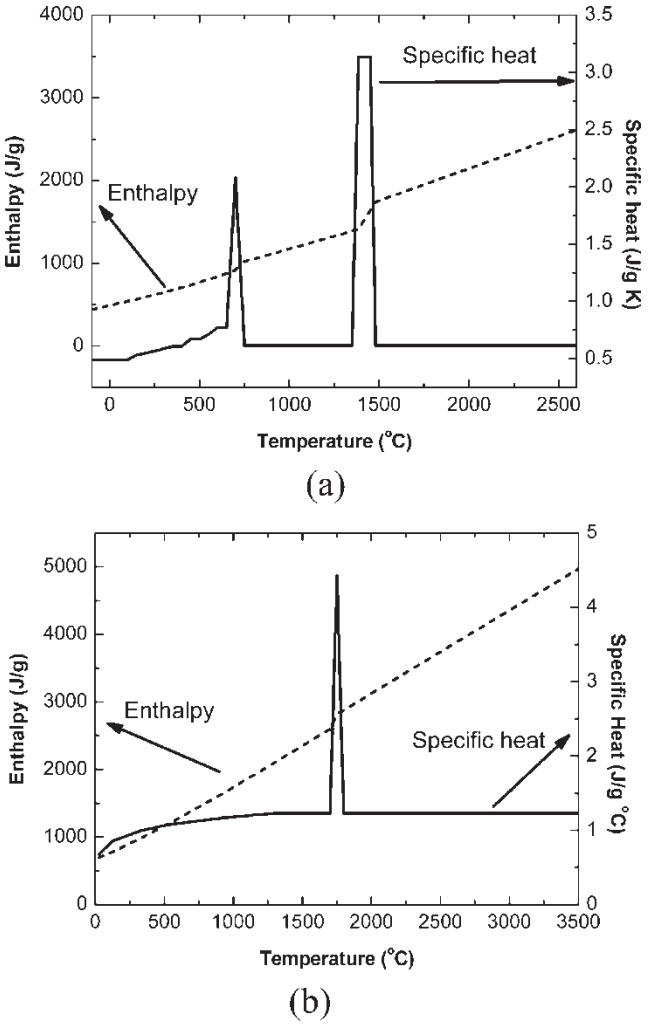

Fig. 3 Enthalpy and specific heat of (a) steel and (b) silicon sand

initial and boundary conditions were supplied for each stage.

2.3.1 Preheating and tapping stage

The preheating and tapping stage encompasses the time period before liquid metal is introduced into the cavity. The initial temperature of the rail and the mould is assumed to be the ambient temperature. During the period of preheating, a steady heat flux was supplied to the rail end exposed to the preheating flame. The magnitude and spatial distribution of the heat flux were estimated from temperature measurements on the rail, as will be explained later in section 3. For the mould interior surface, a convective type condition was applied using $h = 0.01$ W/cm^{2}K with a reference temperature of 2000 °C. A convective heat transfer coefficient of $h = 0.002$ W/cm^{2}K was also applied on the outside surface of the sand mould with respect to the ambient

temperature. Similarly, a temperature-dependent heat transfer coefficient was applied to the rail surface, which varied from 0.0007 W/cm^{2}K at the low temperature end to 0.0013 W/cm^{2}K at the high temperature end. No heat loss was assumed at the mould bottom. After preheating was complete, the heat-input flux on rail end and the convective heat transfer on the mould interior surface were replaced by an adiabatic condition. This simplified boundary condition during the tapping period can be justified by the limited convection that occurs in the weld cavity.

2.3.2 *Solidification stage*

The solidification stage encompasses the time period after liquid metal is introduced into the weld cavity. The initial temperature field for the rail and the mould was obtained from the preheating and tapping simulation. The initial liquid temperature was determined from the peak temperature measured in weld cavity, which varied vertically along the y-axis and horizontally along the x-axis (Fig. 1). It was assumed that no temperature gradient was present along the z-axis in the weld cavity because of the relatively small dimension of weld gap in this direction.

3 VERIFICATION OF HEAT TRANSFER MODEL BY LABORATORY THERMITE WELDING

3.1 Laboratory thermite welding procedure

Full-scale laboratory thermite welding was conducted in the Newmark Civil Engineering Laboratory at the University of Illinois at Urbana-Champaign (UIUC). The parent rail used in welding was a control-cooled 136 lb rail manufactured by the Colorado Steel Company in August 1993. Orgo-Thermit SkV standard thermite welding kits and procedures were used in this study. The chemical analyses for the rail and weld metal are given in Table 1. There is no substantial difference in composition between rail and weld metal, except that the Al content of weld metal is much higher (Table 1).

Two pieces of 1-m long rail were lined up and placed on a support. The weld ends were square-cut with an abrasive rail saw. The distance between two butted rail ends (~25 mm) was measured at the rail base, web, and head prior to the installation of weld mould. The side wall of the rail web and base at the rail end was cleaned to remove surface rust and grease before welding. Then, the weld mould was mounted on the rail and visually centred about the weld centreline. After the weld mould was secured, luting sand was carefully packed around the side and bottom of mould to achieve a liquid-tight seal for the weld cavity.

After completing the setup, the weld cavity was preheated with a slightly reducing propane–oxygen flame. The pressures of oxygen and propane gases were controlled at 65 and 15 psi, respectively, throughout the preheating process. The preheating times varied in different experiments, except for weld F in which no preheating was provided. After preheating, the loaded welding crucible was put in place and centred over the opening of the weld cavity. Then thermite charge was ignited, and the liquid metal was poured into the weld cavity. The time period between the end of preheating and the beginning of pouring is defined as the tapping time. Both the preheating time and the tapping time were measured for each laboratory weld from video tape and are summarized in Table 2. After pouring, the welds were allowed to cool for 1–2 min before the mould shoe, the weld top, and the risers were removed.

Table 1 Chemical compositions of parent rail and completed thermite weld (wt%)

	C	Mn	P	S	Si	Ni	Cr	Mo	Cu	Al
Rail	0.8	0.8	0.02	0.02	0.16	0.01	0.05	0.01	0.02	0.006
Weld	0.7	0.8	0.024	0.006	0.23	0.02	0.04	0.01	0.04	0.3

3.2 Temperature measurement during welding

Holes were drilled in one piece of the rail at different locations to accept thermocouple probes. Exposed K-type thermocouples (Chromel–Alumel) with ceramic insulators were used for rail temperature measurement. The tips of thermocouples were spot-welded into the holes to ensure good thermal conduction. Four pairs of C-type thermocouple probes (W5Re–W26Re) were installed at different locations along the centreline of the weld cavity to measure the weld metal temperature. Small grooves were cut on the weld mould to accommodate thermocouple wires running through the mould wall. A national instrument SCXI multi-channel system was used to collect data during welding. The

Table 2 Welding conditions of the laboratory thermite welds

	Distance between rail ends (mm)			Weight of charge	Preheating	Tapping	Pouring
Weld	Head	Web	Base	(kg)	time (s)	time (s)	time (s)
C	27	28.6	30.2	14.34	289	76	8
D	28.5	27.8	28	14.34	302	62	5
E	28	29	30.5	14.31	380	70	6
F	29	27	25.5	14.35	0	0	7
G	27	26.8	26.5	14.33	350	71	5
H	30	28	27	14.34	467	86	7

temperature variation at the cold junction was monitored and used to compensate the temperature readings in rail and weld metal.

A typical temperature measurement is shown in Fig. 4 for the rail base. The thermocouples at the weld centre were exposed to the propane–oxygen flame directly. Because of the unstable nature of fuel–gas combustion, fluctuations can be seen in the temperature history curves at the weld centre during preheating. The pouring of liquid metal caused a sharp increase in the rail end temperature. At around 800 s, the slag pans and mould shoes were removed, and the temperature readings beyond this time may have been influenced by these mechanical operations.

3.3 Assessments of preheating heat-flux profiles and initial liquid temperatures

To successfully simulate heat transfer in the laboratory welds, two important pieces of information are needed. One is the preheating heat-input profile, which is the required boundary condition of the preheating stage, and the other is the initial liquid temperature profile, which is needed for the initial conditions of the solidification simulation. Temperature measurements in the rail and in the weld centre were used to determine these quantities.

3.3.1 Preheating heat-input assessment

The preheating heat-input profile was estimated using the temperature measurements in the rail prior to pouring. The procedure of heat-input assessment is as follows. A preheating simulation was first performed with an assumed heat-flux profile on the rail end. Then, the calculated temperature history results were plotted and compared with the experimental measurements. On the basis of this comparison, the assumed heat-flux profile was adjusted and used for the next round of simulations. This process was repeated several times until a close match was obtained between the simulation and measurement. The heat-flux profile was then declared to be the preheating heat-input profile for that laboratory weld and used in the corresponding heat transfer simulation.

Figure 5 is a comparison between experiment and simulation using the estimated heat-input profile. Generally, the simulation results were in good agreement with temperature measurements. In some locations, the calculated rate of temperature rise is slightly different from the measured values.

3.3.2 Initial liquid temperature assessment

The initial liquid temperature for solidification simulation was also obtained from the experimental measurements. As the liquid temperature measured in the weld chamber was not uniform throughout the weld cross-section, the peak temperatures were plotted against the distance from rail base. For each laboratory weld, a polynomial curve through the measured peak liquid temperature was defined as the profile of the initial liquid temperature and was used for the solidification simulation for that particular laboratory weld.

3.4 Comparisons between laboratory thermite weld and the simulations

3.4.1 Temperature history

With the determined preheating heat input and initial liquid temperature profiles, the heat transfer problem in laboratory welds can be solved numerically. Combining the results of preheating, tapping, and solidification, the predicted temperature history curves can be compared with measurements in the laboratory welds. Because of the way the preheating heat-flux profile is obtained, the simulation results

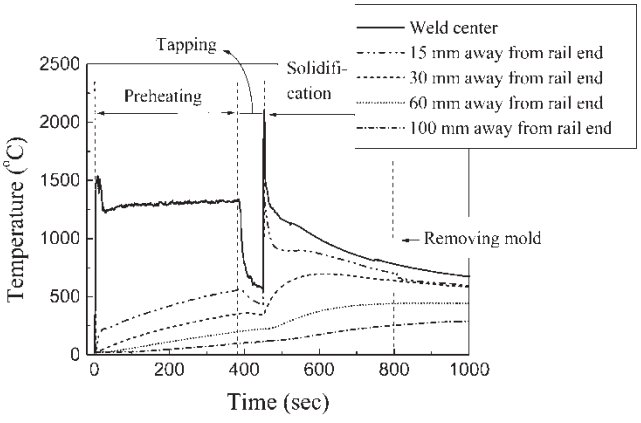

Fig. 4 Typical temperature measurement in the rail base of a laboratory weld

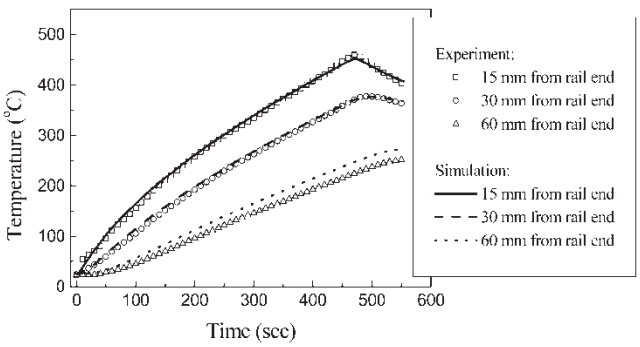

Fig. 5 Comparisons between measured and calculated rail temperature with the estimated heat input profile in the rail head (laboratory weld H)

during the preheating and tapping stage agreed reasonably well with the experimental measurement. The comparison of temperature history during the solidification stage is actually a more critical test for model verification. For this reason, only the temperature history is compared in the solidification stage. Figure 6 is an example of this comparison in laboratory weld H. Two points need to be clarified for this figure.

1. In the figure, only 'good' temperature measurements were plotted with the corresponding simulation results. Although many thermocouples were mounted on the rail and in the weld chamber for each weld, not all of them survived the intensive heat or mechanical operation during the welding. Some of the thermocouples (mostly those close to the rail end) were simply melted or detached from the rail during the welding and gave incorrect readings. These measurements were ignored in the temperature history comparisons.
2. Once the liquid metal was poured into the weld cavity, the weld was allowed to cool undistributed for several minutes. Then, the weld was stripped by knocking off the weld mould, cutting the weld top and removing the risers. These operations may or may not break the thermocouples, but certainly the cooling boundary conditions were changed significantly. Therefore, the temperature readings after this point do not usually agree with the simulations. The starting time of these operations was obtained from the video recording of each laboratory weld and is marked on the comparison figures accordingly.

Figure 6 shows an adequate agreement between experiment and simulation at most thermocouple locations in laboratory weld H. Similar results are also obtained in other laboratory welds. Generally, the predicted temperature history curves match better with the experimental measurements at the locations far away from weld gap. The small differences between experiment and simulation may be attributed to simplifications or inaccuracies in the initial and boundary conditions in the model.

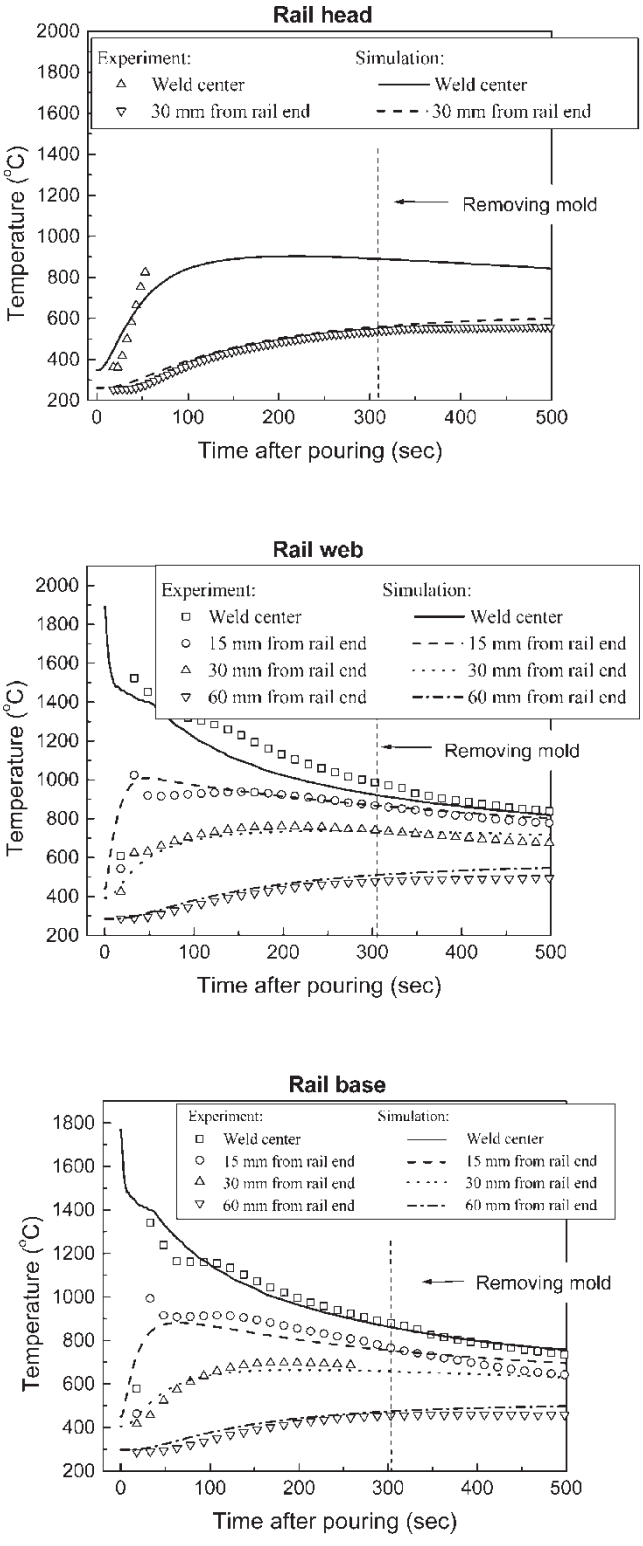

Fig. 6 Comparisons of temperature history curves between simulation and experiment in weld H

3.4.2 Weld deposit and HAZ profiles

Using the heat transfer model, isotherms of different temperatures can be obtained at any given time in a thermite weld. If a physical phenomenon has a certain characteristic temperature, the isotherm of this temperature can be used to represent the occurrence of this physical phenomenon. For example, if it is assumed that the liquid–solid interface has a certain temperature (solidus), then this isotherm can be plotted at different time steps to illustrate the dynamic motion of the solidification front. The furthest location the isotherm of solidus moves into the rail is therefore the profile of weld deposit. Similarly, the profile of the HAZ (whose outermost

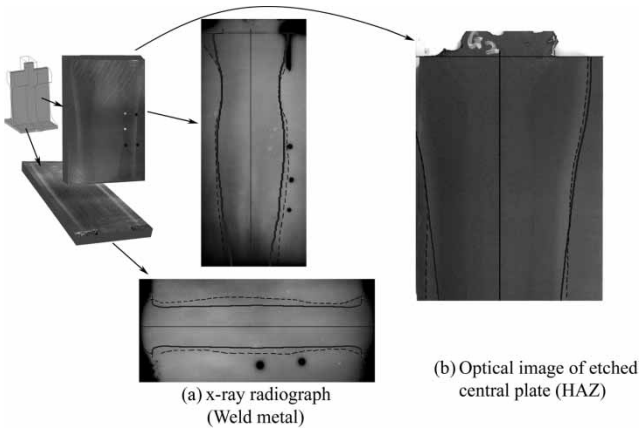

Fig. 7 (a) Comparison of the weld deposit profiles in the rail web and base for weld G; (b) comparison of the HAZ profiles in weld G (the dashed lines are the observation, and the solid lines are the predictions)

boundary is denoted by the eutectoid temperature) can also be determined from the model.

To compare the predicted and the actual weld deposit and HAZ profiles, laboratory thermite welds were cut off from parent rail and sectioned longitudinally in the rail web and head and horizontally in the rail base, as shown in Fig. 7. The obtained plates were lightly etched with Nital (2 per cent nitric acid with ethanol). The profile of HAZ can be readily viewed on the etched surface, but the contrast of weld deposit is relatively poor in some samples. A metallurgical surface finish would be required for a good observation of the profile of weld deposit. As the surface area of the sectioned rail plate is very large (more than 250 cm^2 in the case of the longitudinally sectioned plate), the normal metallurgical polishing becomes time consuming. To characterize the weld deposit profile quickly, radiography is used to determine the boundary of a weld deposit. Because of the difference in density (due to the presence of microporosity and inclusions), the weld deposit appears darker and can be easily identified on a radiograph, as shown in Fig. 7(a) (the black circles on the left side of the image are the thermocouple holes).

In Fig. 7(a), the predicted weld deposit profile is indicated as solid lines, and the observed weld deposit profile is highlighted by dashed lines. When the centreline of the predicted weld deposit profile was lined up with the estimated centreline on a radiograph, a fairly good match was found in most areas. Figure 7(b) shows the comparison of HAZ profiles in the same laboratory weld. Again, a good match was found between the observed and predicted weld profiles. Additional comparisons of weld deposit and HAZ profiles for other laboratory welds give similar results. The difference between the predictions and observations for each laboratory weld was calculated and listed in Table 3. A positive number indicates the predicted profile is narrower than the experimental measurement. In most areas, the predictions agree with the observations reasonably well.

4 DISCUSSION

4.1 Preheating heat-input profile

Figure 8(a) summarizes the estimated preheating heat-input profiles for all laboratory welds, except weld F. The horizontal axis in the figure is the preheating flux, and the vertical axis is the distance from the rail base. In all laboratory welds, the lowest heat-input flux was always at the rail head, and the peak-heat-input flux was in the rail web or the rail base areas. The consistent positioning of the preheating torch for each laboratory weld is responsible for this general profile. However, a fairly large variation can also be seen in the estimated preheating heat-input profiles. The inconsistency of preheating heat-input profiles among different welds seems not to be correlated with the differences in the preheating time and suggests that the heat flux pumped into the rail end is not

Table 3 The predicted and measured weld deposit and HAZ width in laboratory welds

		Weld C			Weld D			Weld E			Weld F			Weld G			Weld H		
Weld sample		E[a]	S[b]	D[c]	E	S	D	E	S	D	E	S	D	E	S	D	E	S	D
Weld deposit width (mm)	Centre of rail head	46	38	8	52	38	14	33	39	−6	32	31	1	40	42	−2	38	43	−5
	Centre of rail web	49	46	3	47	41	6	47	42	5	40	37	3	47	47	0	46	43	3
	Web/base transition area	43	34	9	36	33	3	34	31	3	27	30	−3	35	32	3	31	32	−1
HAZ width (mm)	Centre of rail head	113	113	0	99	108	−9	98	110	−12	78	90	−12	120	117	3	116	113	3
	Centre of rail web	95	92	3	84	81	3	85	77	8	67	57	10	96	97	−1	96	87	9
	Web/base transition area	92	84	8	75	73	2	81	66	15	58	41	17	90	82	8	85	78	7

[a]E, experimental measurement; [b]S, simulation result; [c]D, difference, E − S.

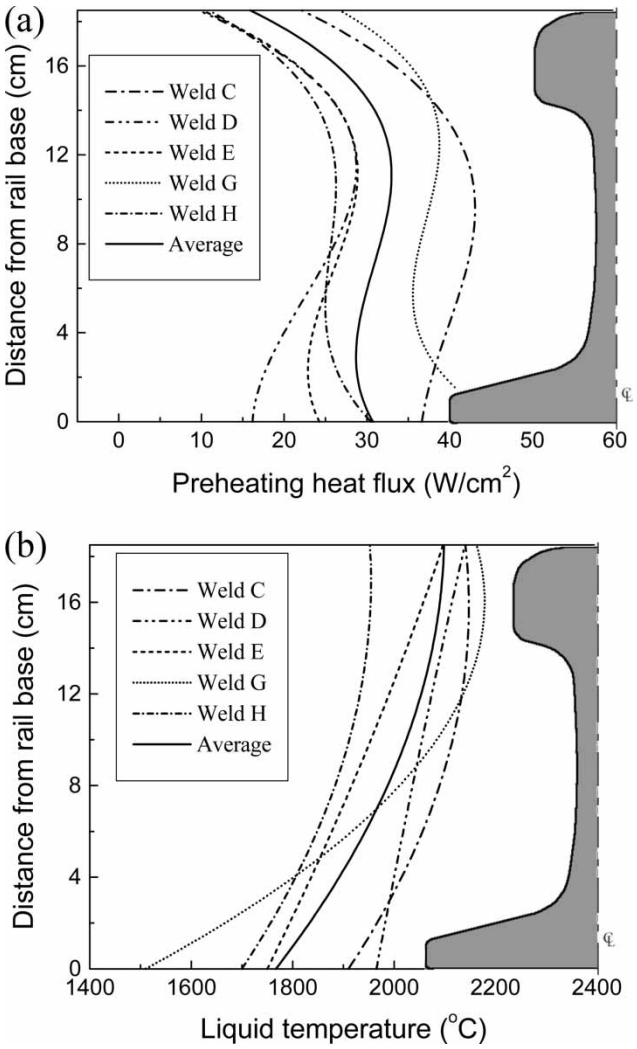

Fig. 8 (a) Preheating heat input and (b) initial liquid temperature used in simulations for laboratory thermite welds (weld F is not included in the averages)

identical in each case, even though the same gas pressures (65 psi for oxygen and 15 psi for propane) and nominal torch position were used. It is possible that controlling the gas pressure by the regulator mounted on the gas tanks is not accurate enough to allow a reproducible preheating condition in different laboratory welds. A gas flow control through flow meters mounted close to the preheating torch might produce a more consistent preheating condition.

4.2 Initial liquid temperature profile

Figure 8(b) shows the initial liquid temperature profiles measured in the laboratory welds. The highest liquid temperature was always found in the rail head, whereas the lowest liquid temperature was in the rail base. The lower liquid temperature in the rail base may be attributed to the heat exchange between the liquid metal and mould wall along the feeding path. During thermite welding, the liquid metal is poured into weld chamber from the top opening and hits the bottom of the weld mould first. Because of the cooling by the cold mould wall, the liquid metal poured in initially (the bottom layer) is cooler than the liquid metal that follows (the upper layer). Thus, a lower liquid metal temperature would be expected in the rail base. As a result, an increasing temperature gradient from the rail base to the rail head is formed in liquid metal after pouring.

4.3 The relative importance of welding parameters on thermal conditions

All welding parameters influence the thermal conditions during the thermite welding process; however, some of them have a stronger effect than the others. To determine the relative importance of a welding parameter, a series of thermal simulations were carried out using the heat transfer model. The predicted weld deposit profiles, the isotherms at the end of solidification, and solidification time were used as benchmarks for comparing the different thermal conditions resulting from simulations.

The welding parameters to be considered are listed in Table 4, and the typical values for a standard thermite weld are indicated. Some welding variables, such as the preheating time and weld gap, are adjustable during welding. The effects of these parameters were explored by varying them around their standard values. Other welding parameters, such as the initial liquid temperature and the preheating heat-flux profiles, are beyond control in current thermite welding practice, so the average values of these parameters and their variations found in the laboratory welds were considered. Figures 9(a) and (b) show the average profiles and variations in preheating heat flux and liquid temperature used for studying their influence on thermal conditions.

The simulation results are presented in a series of images in which the influence of preheating time

Table 4 Welding parameters and their typical values for a standard thermite weld

Weld gap	25 mm
Preheating time	5 min
Preheating heat-flux profile	Curve A (Fig. 9(a))
Tapping time	60 s
Average initial liquid temperature	2050 °C
Initial liquid temperature profile	Curve a (Fig. 9(b))
Ambient temperature	25 °C

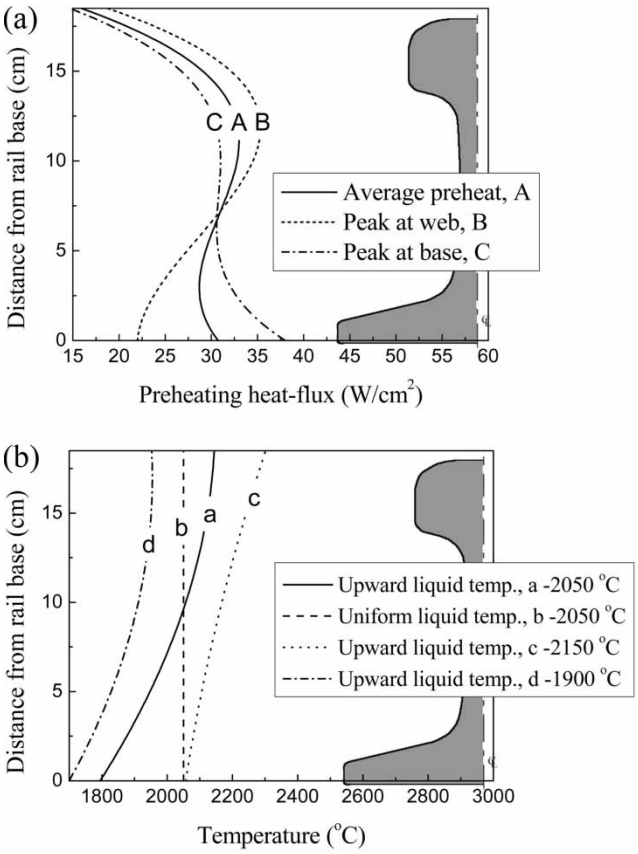

Fig. 9 (a) Preheating heat-flux profiles (curve A is the typical preheating heat-flux found in the laboratory welds, and curves B and C have the same integration area as curve A along the rail height); and (b) initial liquid temperature profiles (curve a is the typical liquid temperature profile found in the laboratory welds, and curve b has the same average temperature as curve a; curves c and d have different average temperatures, but retain the same upward temperature profile as curve a)

and weld gap on the thermal condition development is compared (Fig. 10). In each image, the weld deposit is illustrated by the shaded region on the left, and the edge of the mould collar is marked by a dashed line. The isotherms at the moment when the material in the weld centre 10 mm below the rail head surface solidifies are on the right of each image. The liquid and mushy (partially solidified) zones are also illustrated on the right of each image with different grey scales. The solidification time, which is defined as the time elapsed from pouring to the moment when the weld centre at 10 mm below the rail head surface freezes, is an indication of the rate at which thermal conditions develop in the given thermite weld.

In Fig. 10, images having the same weld gap are arranged in columns, and the images having the same preheating time are in rows. As expected, a longer preheating time leads to a slightly wider weld deposit and a longer solidification time. In contrast, increasing the weld gap can considerably widen the weld deposit and delay the solidification time. It is noted that the increase in weld deposit width is not only due to an enlarged distance between original rail ends, but also due to an increased penetration by liquid metal into the rail ends (the weld deposit profile is closer to the mould collar edge). Hence, although the effects of increasing preheating time and enlarging weld gap are similar, the weld gap is a much more influential welding parameter. Similar analyses were conducted for the other welding parameters, and estimations of their inference based on the benchmarks (weld deposit width, solidification time, and isotherms at the end of solidification) are listed in Table 5.

For the seven welding parameters examined, the tapping time, preheating profile, and ambient temperature have a weak effect on the thermal conditions developed in thermite welds. Preheating time has a moderate influence on the thermal conditions. A relatively stronger influence can be seen for the average liquid temperature and the liquid temperature profile. The most significant welding parameter for the thermal condition development is the weld gap. The variation of weld gap produces a considerable difference in thermal conditions. Because of the strong effect of weld gap, the weak and moderate effects caused by the variations of other welding parameters, such as ambient temperature and tapping time, are effectively eliminated in a wider-gap weld; the effects caused by the other more influential welding parameters, such as initial liquid temperature and its distribution, are also significantly reduced. On the basis of the comparisons among the simulations with different weld gaps, a wider-gap weld is more likely to produce consistent welding results and to be insensitive to variations of the other welding parameters.

5 CONCLUSIONS

1. A finite-element heat transfer model was developed for the standard thermite rail weld. The predicted temperature history curves were verified by temperature measurements in laboratory thermite welds. The heat transfer modelling results were also used to predict the weld deposit and the HAZ profiles. The predictions were in good agreement with the experimental observations.
2. Using both the temperature measurement and the thermal model, the preheating heat-input profiles

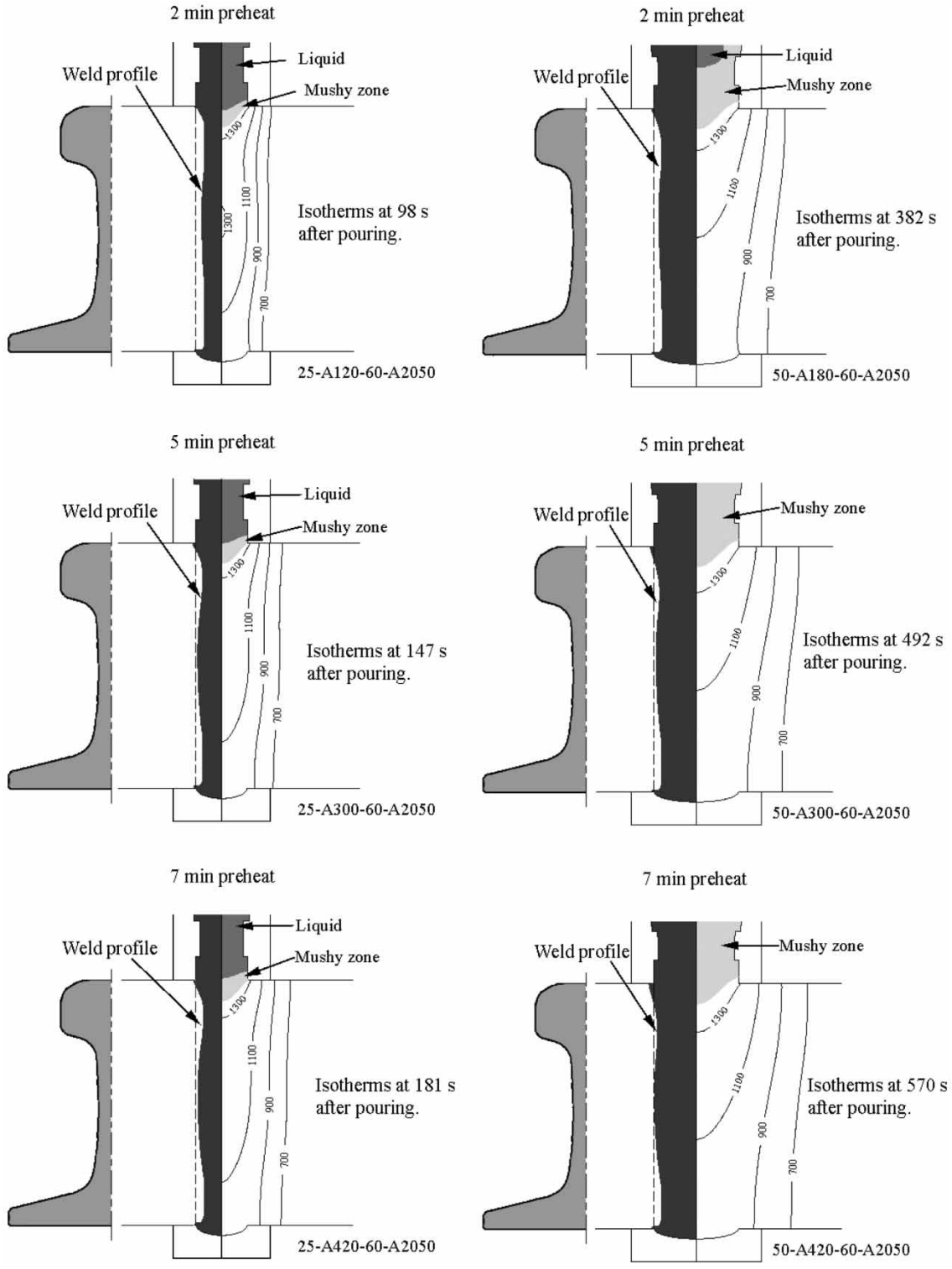

Fig. 10 The influence of preheating time and weld gap (Left column: 25 mm weld gap, Right column: 50 mm weld gap. Isotherms are in °C)

were determined in laboratory thermite welds. The peak preheating heat flux was located in the rail web in most cases and occasionally in the rail base. The preheating heat flux was found to vary considerably in different welds.

3. The liquid temperature distribution after pouring was determined from temperature measurements in weld cavity. An increasing liquid temperature from the rail base to the rail head was found in all laboratory welds.

Table 5 The influence of various welding parameters on thermal conditions

	Effects on			
Welding parameters	Weld deposit width	Weld deposit shape	Temperature gradient	Solidification time
Preheating time	Moderate	Weak	Moderate	Strong
Heat-flux profile	Weak	Weak	Weak	Weak
Tapping time	Weak	Weak	Weak	Weak
Liquid temperature	Strong	Moderate	Strong	Strong
Liquid temperature profile	Strong	Moderate	Strong	Strong
Ambient temperature	Weak	Weak	Weak	Weak
Weld gap	Very strong	Moderate	Very strong	Very strong

4. The most influential welding parameter for thermal condition in thermite weld is the weld gap. The significance of the other welding parameters is pronounced only if the weld gap is small. For a wider-gap weld, the effects caused by increasing weld gap override the influence of the other welding parameters, and therefore wider-gap welds appear to be less sensitive to chance variations in the other welding parameters and fairly consistent thermal conditions can be obtained.

ACKNOWLEDGEMENTS

The authors would like to thank Joseph Kristan and David Davis of the Association of American Railroads' Transportation Technology Center Inc. and Frik Hefer of Orgo-Thermit Inc. for their interesting discussions throughout this study. Dr Grzegorz Banas, Eric Ross, Jeff Cyre, and Alberto Alvarez-Lozano from the UIUC are also acknowledged for their contributions to the experimental effort. This work was sponsored by the Association of American Railroads Technology Scanning and Strategic Research Programs and the Transportation Research Board High-Speed Rail IDEA Program (HSR-41). The computational work was partially supported by National Computational Science Alliance under MSS030005 N and utilized the IBM P690.

REFERENCES

1 **Hart, R. N.** *Thermit welding process*, 1987 (Lindsay Publications, Inc., Bradely).
2 **Brumbaugh, J. E.** *Welders guide*, 1975, Chapter 10 (Howard W. Sams & Co, Inc., Indianapolis).
3 **Myers, J., Geiger, G. H.,** and **Poirier, D. R.** Structure and properties of thermite welds in rails. *Weld. Res. Suppl.*, 1982, **8**, 258.
4 **Schroeder, L. C.** and **Poirier, D. R.** The mechanical properties of thermite welds in premium alloy rails. *Mater. Sci. Eng.*, 1984, **63**, 1.
5 **Jha, B.** *Thermite welding of rail steel.* PhD Dissertation, Illinois Institute of Technology, 1989.
6 **FIDAP**. *FIDAP User's manual*, 2001 (Fluent Inc., Lebanon, NH).
7 **Pehlke, R. D., Jeyarajan, A.,** and **Wada, H.** *Summary of thermal properties for casting alloys and mold materials.* University of Michigan, Ann Arbor, MI, 1982, Photocopy. Springfield, VA: National Technical Information Service [1983].
8 **FIDAP.** *FIDAP Theory manual*, 1999 (Fluent Inc., Lebanon, NH).
9 **Dantzig, J. A.** Modelling liquid-solid phase changes with melt convection. *Int. J. Numer. Methods Eng.*, 1989, **28**, 1769–1785.
10 **Valencia, J. J.** and **Yu, K.-O.** Thermophysical properties. In *Modeling for casting and solidification processing*, (Ed. K.-O. Yu) 2002 (Marcel Dekker, Inc., New York).

APPENDIX

Notation

C_p	specific heat
h	heat transfer coefficient
H	enthalpy
k	thermal conductivity
$\dot{Q}$	heat generation rate
t	time
T	temperature
ρ	density